Nonlinear Dyn
https://doi.org/10.1007/s11071-022-07864-y

ORIGINAL PAPER

Poincare maps: a modern systematic approach toward obtaining effective sections

Amir Shahhosseini · Meng-Hsuan Tien · Kiran D'Souza

Received: 13 May 2022 / Accepted: 26 August 2022

Abstract Despite its importance and widespread applications, the use of the Poincare map has remained in its rudimentary stages since its proposition in the nineteenth century and there exists no systematic method to effectively obtain Poincare sections. Additionally, and due to its graphical structure, it has previously been very arduous to utilize Poincare maps for high dimensional systems, and two- and three-dimensional systems remain as its sole area of applicability. In this study, a novel systematic geometrical-statistical approach is proposed that is capable of obtaining the effective Poincare sections regardless of the attractor's complexity and provides insight into the entirety of the attractor's structure. The presented algorithm requires no prior knowledge of the attractor's dynamics or geometry and can be employed without any involvement with the governing dynamical equations. Several classical systems such as the Van der Pol, Lorenz, and Rossler's attractor are examined via the proposed algorithm and the results are presented and analyzed.

Keywords Poincare map · Computational nonlinear dynamics · Applied mathematics · Strange attractors · Chaos

1 Introduction

Poincare maps are capable of providing insightful graphical presentations of the qualitative behavior of dynamical systems and ergo, are widely utilized in the analysis of nonlinear dynamics. The simplicity of the fundamental idea behind Poincare maps, intertwined with its wide spectrum of applications, makes it one of the critical tools in analyzing nonlinear dynamical systems. Stability analysis of dynamical systems [12], identification of quasiperiodic orbits [5,17], enhancement of the quality of control algorithms [19], identification of limit cycles [16] and, the determination of the regime of motion [2] are considered to be the main utility of this tool.

Despite their importance and significant applications, there lacks a universally apposite and systematic method for the attainment of these maps. In fact, the Poincare maps of the literature are always obtained using rather arbitrary Poincare sections that are drawn based on the visual perception of authors from the tra-

Supplementary Information The online version contains supplementary material available at https://doi.org/10.1007/s11071-022-07864-y.

A. Shahhosseini · K. D'Souza (✉)
Department of Mechanical and Aerospace Engineering, The Ohio State University, Columbus , OH, USA
e-mail: dsouza.60@osu.edu

A. Shahhosseini
e-mail: shahhosseini.3@osu.edu

M.-H. Tien
Department of Power Mechanical Engineering, National Tsing Hua University, Hsinchu City, Taiwan (R.O.C.), China
e-mail: mhtien@pme.nthu.edu.tw

Published online: 25 September 2022

jectories of interest. This lack of systematic methodology can cause issues and ambiguities in the analysis of the behavior of complicated and unconventional nonlinear systems since different Poincare sections can highlight different behaviors. In fact, it is even possible to fabricate systems that demonstrate periodic behavior for certain Poincare sections while illustrating chaotic behavior for alternative Poincare sections. Additionally, due to their *graphical* nature, Poincare maps have not previously been able to be used to examine the behavior and dynamical characteristics of high-dimensional systems. To resolve these fundamental deficiencies and limitations, a new approach toward the efficient obtainment of effective Poincare sections for general n-dimensional systems is required.

To propose a standard universal method that can provide effective Poincare sections, the fundamental idea behind Poincare maps should be revisited. By defining a section and obtaining the crossings of the trajectory with the section, a Poincare map attempts to identify the dynamical properties of the trajectory, or more accurately, the attractor that is governing the motion. The structure of the attractor can consist of one rotary flow (such as the periodic motion of a linear harmonically excited mass spring damper system), two flows (such as the Lorenz strange attractor), or more flows (such as the Rabinovich–Fabrikant attractor). Nearly all stable deterministic dynamical systems, from periodic to chaotic, usually revolve around one or more specific regions in their trajectory spaces due to the boundedness of their motion. The part of the trajectory, in trajectory space, that revolves around a specific region is called a rotary flow in this paper. To examine the dynamical properties of the attractor with some confidence, it is essential to examine each rotary flow of the attractor in detail. Additionally, examining regions of each rotary flow with the highest *concentration* of trajectory data will be particularly beneficial since it can provide more information on the behavior of the system when compared to alternative regions. Consequently, a multi-section approach is critical as the number of rotary flows and dimension of the system increases.

The algorithm of this paper relies upon a geometrical-statistical approach for the identification of the principal portions of the trajectory to find adequate Poincare sections. The first step of the algorithm is to calculate the centers of curvature (COC) corresponding to each point of the trajectory to identify the rotary flows of the attractor. This is motivated by the fact that an aggregation of the COCs manifests the central region of the rotary flow. Next, a clustering process is applied to the COC data to identify the number of clusters (which is the same as the number of rotary flows) and their corresponding centroids, the *primary centroids*. After the identification of the rotary flows and their centroids, which are in fact the centroids of the center of curvature data, the trajectory is partitioned into subsets of the original space using hyperplanes that are drawn based on statistical orientation criteria. A clustering process is performed on the trajectory data in each of those subsets of the original space to identify the major components of the flow and their corresponding centroids, the *secondary centroids*. The optimal Poincare sections of this algorithm are those that connect the primary centroids to secondary centroids while maximizing the orthogonality of the Poincare section with the flow in an optimization problem.

In addition to its *systematic* approach, the advantages of the proposed algorithm are twofold. First, owing to the description of the trajectories in Euclidean metric space, a geometrical logic can be extended to high dimensional systems and is generalizable. Furthermore, the geometrical essence of the algorithm prevents the necessity of rigorous feasibility conditions that will inevitably arise when using analytical approaches. Second, this geometrical foundation enables the attainment of adequate Poincare sections regardless of the level of sophistication of the governing dynamics since the algorithm solely concentrates on the geometry of the problem.

To demonstrate the effectiveness and capabilities of the proposed algorithm, several complicated classical systems are examined. This study begins with a concise explanation of the algorithm and then applies it to the Duffing oscillator [10], the Van der Pol oscillator [8], a PWL oscillator [15], a Lorenz attractor [18], a Rabinovich–Fabrikant attractor [3], and Rossler's three- and four-dimensional attractors [1,13] to systematically obtain effective Poincare maps. It is observed that the proposed algorithm functions effectively without any modifications for all the aforementioned systems without the necessity of any prior knowledge of their dynamics or the geometry of their trajectories.

2 Methodology

To gain an understanding of the structure of dynamical attractors, Poincare maps are often utilized. The veracity of this understanding is based upon the appropriate selection of sections for the Poincare map that must cross through the pivotal areas of the attractor. Before delving into the definition and the procedure of identifying these areas, it is important to discuss the logic behind their pivotal importance. By correctly detecting these few areas, it is possible to moderately approximate the general qualitative geometry of the attractor to the point of rough reconstruction. Consequently, by meticulously analyzing the attractor using these areas, the properties of the structure can be recognized. Figure 1 demonstrates the general procedure of the proposed algorithm graphically. The algorithm consists of a primary cluster analysis on the centers of curvatures of trajectory data, followed by the partitioning of its space into apposite subsets of the original space. After obtaining the subsets of the original space, a secondary cluster analysis is performed on the trajectory data to identify zones with highest data concentration. The algorithm provides its sections by obtaining the plane (or hyperplane in case of high-dimensional systems) that crosses through these zones while maximizing orthogonality with the trajectory data.

2.1 Importance of centers of curvature

The first and most important pivotal area is related to the COCs. A cluster of COCs suggests the rotation of the attractor about that specific area and ergo, indicates the distinct existence of a rotary flow. The quantity of the COC clusters can determine the number of existing rotary flows. The corresponding cluster centroids, named *primary centroids*, are used for the partitioning of the n-dimensional space into n-dimensional subsets of the original space for further manipulation. Additionally, the inclusion and recognition of primary centroids in constructing the Poincare sections guarantees the examination of every rotary flow.

The partitioning of the n-dimensional space into n-dimensional subsets of the original space is performed using the proposed uninvolved statistical method of this study to simplify the determination of zones with a high concentration of trajectory data. Note that the n-dimensional space is partitioned via apposite hyperplanes that each cross through one primary centroid and in fact, cut the *central area* of their corresponding rotary flow. Figure 1e demonstrates this partitioning.

The last pivotal area is the zones with a high concentration of trajectory data in each partition. It is important to note that identifying the centroids of trajectory data clusters in each partition facilitates the analysis of the structure of the attractor because a section that goes through such a point provides maximal crossings and consequently, can provide maximal information about the attractor's behavior. Figure 1g illustrates the secondary centroids in every partition.

2.1.1 Calculation of centers of curvature

The foundations of this algorithm rely on the computation and utilization of the COCs. Although there are a variety of methods capable of computing the COC of a known curve, this section will briefly discuss two numerical approaches. The first approach, which was used in this work, uses n points in the n-dimensional space, to obtain the hyperplane they can define, and then searches for a point on the hyperplane that is equidistant to the n points. To facilitate the understanding of this methodology, consider a trajectory in 3D space. Using this approach, at every instance, 3 consecutive trajectory data points are considered and the corresponding plane that includes all three points is computed. Moreover, in that particular plane, the location of the center of a circle that includes all three points is calculated. The center of that circle, which lies inside the aforementioned plane, is the COC of the 3 data points of interest.

An alternative approach, which is similar to the one used herein, uses $n + 1$ points instead and does not define a plane. It tries to locate a point that is equidistant to the $n + 1$ points in the n-dimensional space. In 3D, this corresponds to finding the center of a sphere that includes the 4 data points on its surface. This approach is less suitable for trajectories that have a planar rotation structure (e.g., the Lorenz attractor) but works well when the attractor's rotary flows are not flat. All the corresponding computations can be done using a least-square optimization. Due to using an optimization algorithm, the process of finding the correct COC is tightly related to the quantity and the distance of consecutive trajectory points. A trajectory with rather distant consecutive data will usually result in poor approximations of COCs.

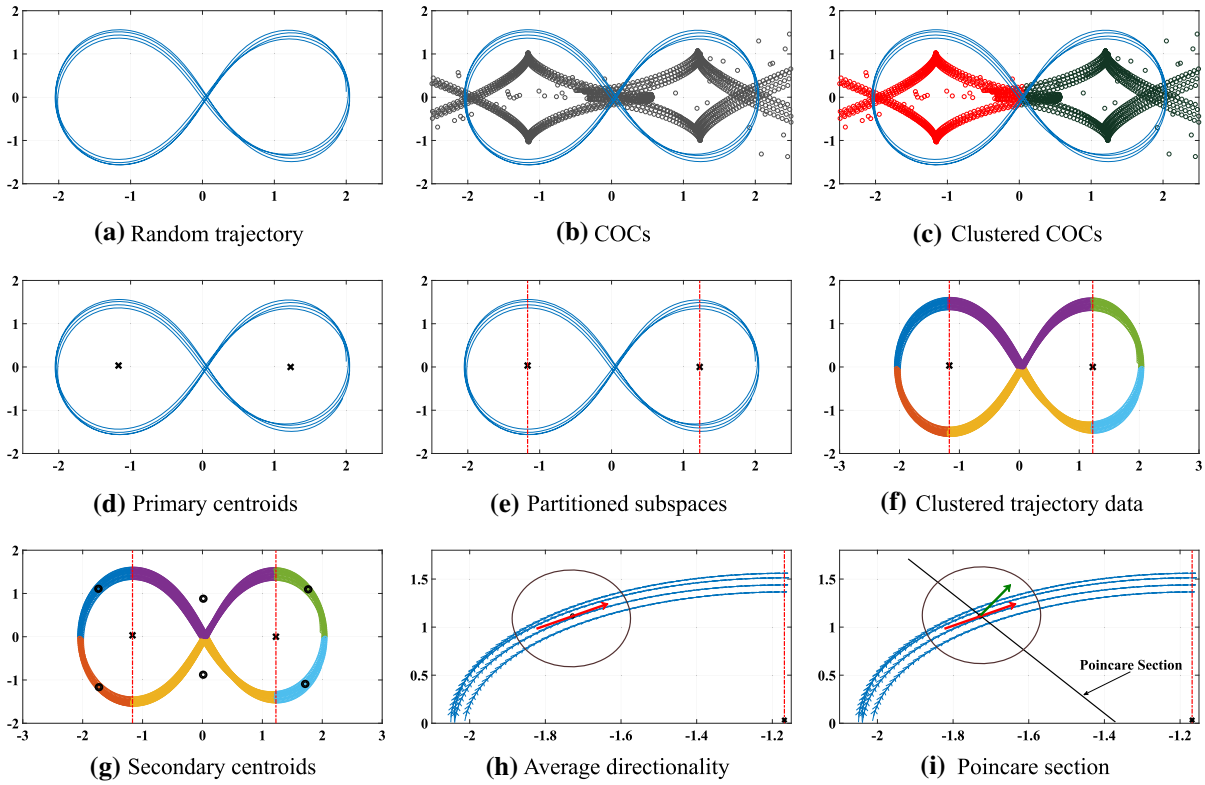

Fig. 1 The schematic procedure of the proposed algorithm for a generated trajectory. Each subfigure demonstrates one of the major steps in obtaining the optimal Poincare sections: **a** the generated trajectory; **b** the COCs are computed and plotted as grey dots with those within the limiting bounds of the trajectory stored for further computation; **c** a clustering algorithm is performed and the COC data are categorized into two clusters where each cluster is related to one rotary flow; **d** the centroid of each of the clusters is identified, and each centroid roughly corresponds to the center of its corresponding rotary flow; **e** based on this study's statistical method, the trajectory space has been partitioned into subsets of the original space to facilitate the rest of the process; **f** the trajectory data, in each partition, is segregated into clusters using an additional cluster analysis to identify the critical zones of trajectory data; **g** the centroids of the trajectory data, referred to herein as the secondary centroids, are computed for further analysis; **h** the trajectory data in the proximity of the secondary centroids are selected and their average directionality is computed; **i** the Poincare section is chosen so that it attempts to go through the secondary centroid while being as close to its corresponding primary centroid as possible and having a normal vector that matches the average directionality vector of the proximity data. Note that one Poincare section is indicated in (**i**) and there would be 5 additional sections, one for each of the critical zones indicated in (**f**)

It is important to reiterate that this study attempts to use the most basic possible methodologies in its structure. This demonstrates the algorithm's effectiveness even when employing basic methodologies. However, more advanced and problem-oriented methodologies can readily be applied in the algorithm to improve its output.

2.1.2 Cluster analysis of centers of curvature

Clustering is referred to the process in which data points are segregated into groups that within each, they are more similar to each other when compared to other groups. Its final goal is to form groups with similar traits, properties, or characteristics from unsorted data.

In this study, clustering is used to segregate the COC data points into different groups to identify the quantity and center of rotary flows. Additionally, and after partitioning the n-dimensional space into apposite n-dimensional subsets of the original space, clustering is performed on the trajectory data to find the pivotal areas of the flow with a high concentration of data.

The clustering method that is employed in this study is *k-means* [11], which is one of the most basic clustering algorithms found in the literature. It attempts to partition data into k clusters by assigning each data to

the cluster with the closest mean. Due to its simplicity, the clustering results are not always optimal.

An additional issue in cluster analysis lies in the determination of the optimum number of clusters. Several methods exist to find the optimum number of clusters using the *k-means* clustering algorithm. In this study, the *silhouette* score interpretation is used to find the optimum number of clusters.

The optimal number of clusters can be calculated before the execution of the cluster analysis using different methodologies such as the silhouette method, the elbow method, the gap statistic, etc. Although these methodologies have different approaches in obtaining the adequate number of clusters, their results are usually in close match with each other when it comes to continuous data. In case of high-dimensional systems, the methodologies would work without any theoretical issues since the underlying principles are independent of dimensionality. Nevertheless, the computational cost of the cluster analysis of high-dimensional systems is rather considerable and therefore, more efficient options should be examined for these cases.

It should be noted that when using optimal cluster number selection algorithms, as described in the paper, the user will not miss any of the key features of the trajectory's dynamics. In contrast, if one were manually choosing the centroids, it is likely one would miss certain regions of the dynamics. However, if only the number of the selected primary centroids are slightly fewer than necessary, one may capture the dynamics if additional secondary centroids are chosen to compensate. Alternatively, upon the selection of more primary centroids, two separate issues might arise. The first issue is that the computational cost of the algorithm will be increased significantly. Additionally, having more primary centroids can be translated into having more partitions and consequently, tighter partitions. The intense tightening of partitions is undesirable since it reduces the amount of data per partition. This can negatively affect the second clustering run (to find the secondary centroids) and therefore, generate inadequate sections. In the case of having only few more primary centroids than the optimal number, no critical issues would arise, but the number of Poincare maps would increase without any additional insight into the dynamics.

Since the ultimate goal of this algorithm is to find where the COCs are concentrated *inside the trajectory*, a limiting bound is introduced to remove COC data that are relatively far from the trajectory. Nevertheless, for some geometrically specific cases, it is possible to have no COC data in the limiting bounds. In that case, it is recommended to use a *coefficient of contraction* that scales the COCs to be in the same order as the trajectory data. In the simulations of this study, the coefficient of contraction is solely used for the PWL system and the rest of the systems function well without using it.

2.2 Partitioning of the center of curvature data

As previously noted, the centroids of the COC clusters are important and signify the centers of the trajectory's rotary flows. Nevertheless, to fully identify the rotary flows and to obtain effective Poincare sections, further information is required. To offer an in-depth analysis of the flows, it is essential to identify the zones with the highest data concentration in each rotary flow. These zones will facilitate the obtaining of the effective Poincare sections since the effective Poincare sections are meant to identify and analyze each and every rotary flow. In fact, an effective Poincare section crosses through both the primary centroid and its corresponding secondary centroid. However, before the secondary centroids can be identified, it is essential to differentiate the rotary flows from each other. This can be done using numerous approaches but, in this paper, a partitioning algorithm is used. This algorithm divides the n-dimensional space into n-dimensional subsets of the original space by introducing hyperplanes that cross through the primary centroids. This partitioning facilitates the identification of the secondary centroids since the cluster analysis that is meant to identify high data concentration zones of each rotary flow is now constrained to be carried out in its corresponding subset of the original space. To elucidate the necessity of this step, the example of Fig. 1 can be revisited. In Fig. 1d the primary centroids are identified, and the centers of the rotary flows are determined. Nevertheless, it is impractical to carry out cluster analysis on the trajectory data as a whole since they would not provide the zones of high data concentration that is desired. In fact, by running the cluster analysis on the trajectory data without partitioning, the secondary centroids will be observed to be very close to the primary centroids, which would not be useful. However, by partitioning the space into adequate subsets of the original space, as illustrated in Fig. 1e, it is possible to segregate the trajectory data and then perform the secondary cluster

analysis. As can be observed from Fig. 1f and g, the results are in agreement with the required objective.

Many algorithms can be used to conduct the space partitioning. This work uses a very rudimentary approach for obtaining the partitioned subsets of the original space to demonstrate the robustness of the proposed methodology.

After the identification of the m primary centroids using the clustering algorithm, the n-dimensional space is partitioned into $m+1$ subsets of the original space using apposite hyperplanes. As previously discussed, each hyperplane goes through a primary centroid but the orientation of the hyperplanes is determined using a simple statistical approach. The idea behind this approach is to avoid having overly compacted partitions with relatively small sizes. This approach ensures that there is enough trajectory data in each partition so that the clustering algorithm can provide meaningful secondary centroids. The approach can be stated as follows. Assume an n-dimensional space. The position of the ith primary centroid can be represented as

$$P_1^i = \{q_1^i \quad q_2^i \quad \dots \quad q_n^i\}, \tag{1}$$

where a subscript of one indicates the centroid being primary and q_j^i specifies the jth coordinate of the ith centroid. To obtain the optimal orientation of the hyperplane in the form of $q_j = c$ where c is a constant, it is possible to introduce the following parameters

$$\begin{aligned} \Delta q_j^i &= q_j^{i+1} \quad - q_j^i, \\ q_j^{dec} &= \frac{max\{\Delta q_j^i\}}{min\{\Delta q_j^i\}}. \end{aligned} \tag{2}$$

Bear in mind that to calculate Δq_j^i, the primary centroids need to be sorted for each j. That is to calculate Δq_1^i, the primary centroids must be sorted based on the numerical value of their first coordinate and so on. This is to ensure that for each coordinate, the primary centroids are evaluated relative to their closest primary centroids. By comparing the q_j^{dec} values, it is possible to obtain the least compacted orientation as

$$\begin{aligned} &\text{Optimum orientation is associated with} \\ &= min\{q_j^{dec}\}. \end{aligned} \tag{3}$$

For example, if the optimum orientation index is $q_j^{dec} = q_1$ then the equation of the partitioning hyperplanes can be defined as $q_{P_1}^{hyperplane} = q_1^1$, $q_{P_2}^{hyperplane} = q_1^2$, etc.. The aforementioned approach is useful when there are more than two primary centroids in the analysis of the trajectory. Nevertheless, in most classical examples (such as the Lorenz attractor) there are only two primary centroids. In that case, the definition of q_j^{dec} changes to

$$q_j^{dec} = \frac{1}{\Delta q_j^1}, \tag{4}$$

and the orientation will be determined as discussed.

To provide a graphical understanding to this orientation criteria, it is beneficial to return to Fig. 1. As it can be observed, the corresponding value of Δq_1^1 is less compacted relative to Δq_2^1, which means that upon partitioning the space using $x = c$ lines, the partitions are less compacted than when compared to $y = c$ lines that go through the primary centroids. This conclusion is illustrated in the computation of q_j^{dec} and the corresponding criteria.

It should be noted that if there are a large number of primary centroids, the proposed methodology might not provide the optimum results and more sophisticated statistical methodologies might be required. Nevertheless, and as observed in the results section, this simple method works very well, even for high dimensional systems.

2.3 Orientation identification of trajectory data in the adjacency of secondary centroids

After obtaining the primary and secondary centroids, it is necessary to connect each primary centroid to the corresponding secondary centroids in its partition to obtain the effective Poincare sections. In general, infinite hyperplanes can be proposed and further information is needed to define the most effective Poincare section. To address this issue, it is desired for the Poincare section to cross through the secondary centroid while maximizing the orthogonality of the section hyperplane with the average flow of trajectories in that area. Therefore, the direction of the average flow in the area adjacent to each secondary centroid is calculated and then used as the normal vector for the Poincare section (which is a plane in 3D systems and a hyperplane in higher-dimensional systems).

Computing the direction of the average flow in the region adjacent to each secondary centroid is not a straightforward task. First, the adjacent region of the

secondary centroid must be defined. In this study, this region is defined to be the space that its Euclidean distance from the secondary centroid is smaller than a predetermined value α. By this definition, for a 3D example, all the trajectory data within a sphere of radius α with its center on the corresponding secondary centroid are included. The radius of this hyperspace (α) is set to be equal to 30% of the length of the partition measured by the beginning of the partition to its end toward the axes determined by the optimum orientation. Bear in mind that this number can be altered as desired by the user, but a much smaller number might fail to capture the entirety of the regional flow and alternatively, a much larger number will include unrelated data. Nevertheless, for agile dynamics, it is recommended to decrease this number to 10-15% as to avoid abrupt directionality alterations of the flow near the secondary centroids. Now, to compute the direction of the average flow vector, the following expression must be maximized.

$$S = \left\{ \sum_{i=1}^{N} |v_i \cdot V| \right\}, \tag{5}$$

where in the above expression, v_i is defined as the vectors that would be created upon connecting consecutive trajectory data in the adjacent region. The vector V is the average directionality vector that is found by maximizing S, and $[\cdot]$ represents the inner product.

To explain this simple methodology, it is beneficial to revisit the objective. It is desirable to obtain the vector that indicates the average direction of the flow near each secondary centroid. By using consecutive trajectory data to create a number of small vectors, the flow near each secondary centroid is now represented by vectors. The inner product of two unit vectors is a measure of their relative orientation. Higher magnitudes of the inner product suggest a similar orientation while lower magnitudes suggest very different orientations. The maximization of S means that the average directionality vector's orientation V is most aligned with the combination of all the vectors forming the flow in the region near the secondary centroid.

2.4 The optimization process of Poincare sections

The simplest way to define a hyperplane is with a normal vector and one point that is on the plane. The average directionality vector can be considered as the normal vector for the Poincare section, however, since the Poincare section should contain two points (both the primary and secondary centroids), in general the Poincare section is overconstrained. Therefore, in this work, an optimization process was used to find the Poincare section. The optimization process searched for the Poincare section that has a normal vector closest to the average directionality vector while having the least Euclidean distance from the corresponding primary and secondary centroids. In different geometries, the degree of importance of each of the objectives is different and consequently, it is rather beneficial to weight the objectives.

This study uses a nonlinear least square algorithm to solve this minimization problem. All the objective functions in this paper are to be minimized and represent a minimization optimization problem. The first objective function is defined as

$$OF^1_{Section} = (V_1^{real} - V_1)^2 + \ldots + (V_n^{real} - V_n)^2, \tag{6}$$

where V_i^{real} denotes the actual normal vector of the Poincare section while V_i shows the average directionality vector obtained from the maximization of expression S. If the secondary centroids are presented as

$$P_2^i = \{w_1^i \quad w_2^i \quad \ldots \quad w_n^i\}. \tag{7}$$

Then the second and third objective functions can be defined as

$$OF^2_{Section} = ((V_1^{real} \times w_1^i) + \ldots + (V_n^{real} \times w_n^i) - D)^2, \tag{8}$$
$$OF^3_{Section} = ((V_1^{real} \times q_1^i) + \ldots + (V_n^{real} \times q_n^i) - D)^2, \tag{9}$$

where D is the constant of the hyperplane if defined as

$$\text{Equation of hyperplane} : a_1x_1 + a_2x_2 + \ldots a_nx_n = D \tag{10}$$

By conducting the optimization to solve for V^{real} and D, the effective Poincare sections in this work were obtained. The Poincare sections of this method are obtained via the minimization of the objective functions of Eqs. (6, 7 8 and9) using a nonlinear solver. However, these minimizations have underlying geometric interpretations. Equation 6 ensures that the normal vector of the hyperplane is as parallel to the local flow of the trajectory as possible to maximize the orthogonality of the resulting Poincare section with the flow. It is known

from elementary geometry that a hyperplane can be uniquely identified if the normal vector and a single point on the plane are known. Nevertheless, in the case of this problem, the methodology attempts to propose a Poincare section that passes through both a primary centroid and a secondary centroid. This is clearly an over-constrained geometrical problem and therefore, the resulting Poincare section is not unique from a rigorous mathematical point of view. However, since a hyperplane that adequately satisfies all these conditions usually exists, it can be argued that the resulting Poincare sections are qualitatively unique but due to the over-constrained nature of the problem and the employment of numerical nonlinear solvers, they might demonstrate slight variations. However, to cope with this issue, it is possible to assign different weights to the objective function (usually assigning a higher weight to Eq. (8) to strengthen the requirement of the inclusion of the secondary centroid) to omit any concerns regarding the computational issues and uniqueness of the obtained Poincare sections.

2.5 Obtaining the Poincare map

After computing the appropriate Poincare sections, it is necessary to obtain the Poincare maps. To do so, the trajectory data are examined to spot intersections with the Poincare sections and upon finding them, a linear interpolation algorithm is used to find out the exact position on the section. To find the intersections, the positions are inserted into the equation of the hyperplane of the Poincare section and its sign is calculated. This is demonstrated as

$$\text{Trajectory Data} = \{y_1 \quad \ldots \quad y_n\} \tag{11}$$

and

$$HS = a_1 y_1 + a_2 y_2 + \ldots + a_n y_n - D. \tag{12}$$

A change in the hyperplane sign (HS) indicates the crossing of the trajectory through the section and consequently, the two points, one on each side of the hyperplane are stored. The linear interpolation algorithm finds a point between these two points that lies on the hyperplane. This is solved by converting this problem into an optimization task. The first objective function for this optimization task can be defined after the proposition of the following parameters

$$B = [y_1^b \quad - \quad C_1, \quad \ldots, \quad y_n^b \quad - \quad C_n], \tag{13}$$

$$A = -[y_1^a \quad - \quad C_1, \quad \ldots, \quad y_n^a \quad - \quad C_n], \tag{14}$$

where y^b denotes the coordinates of the point before the crossing and y^a represents the point after the crossing. The point C is the desired point that lies within the hyperplane and is the rough linear interpolation between y^a and y^b.

$$OF_{Map}^1 = |\frac{A \cdot B}{|A||B|} - 1| \tag{15}$$

This objective function ensures that the crossing point is within the line that passes through points y^a and y^b. The next objective function can be defined as

$$OF_{Map}^2 = |(V_1^{real} \times C_1) + \ldots + (V_n^{real} \times C_n) - D|. \tag{16}$$

This objective function guarantees that the crossing point lies in the previously obtained hyperplane that defines the Poincare section. After obtaining the corresponding crossings, it is required to express C in the coordinates of the hyperplane. This facilitates the graphical representation. For example, assume that the system is 3 dimensional. The Poincare section is a 2D plane in this space but if we look at the coordinates of C alone, three variables can be observed. To resolve this issue, a rotation of the plane is necessary to make the plane parallel to one of the axes and omit the corresponding coordinate. By doing so, in any dimension, the Poincare map is obtained and the problem is solved. Figure 2 provides a schematic overview of the proposed methodology and when combined with the graphical aid of Fig. 1, paints a complete picture of the algorithm's structure.

3 Results

To illustrate the effectiveness and merits of the proposed methodology, numerous classical nonlinear systems with varying behavior are examined. The discussed systems are two, three, and four-dimensional but the methodology also functions for higher dimensions.

3.1 2D attractors and the importance of an adequate section

To demonstrate the capabilities and effectiveness of this methodology, several systems will be studied and the

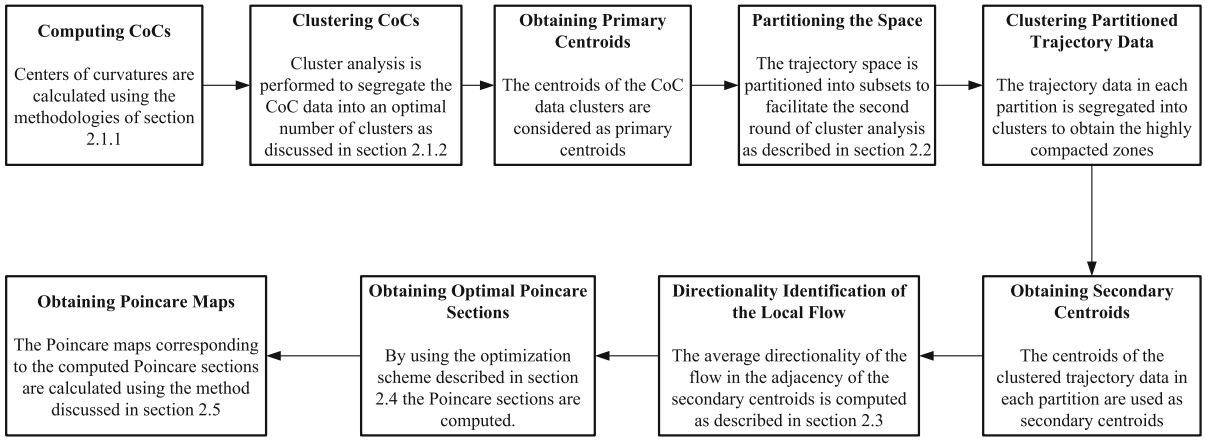

Fig. 2 Schematic view of the structure of the proposed methodology. Each block represents a necessary step in the process of obtaining the adequate Poincare maps. The structure does not rely on any specific computational tools or methods and the details of this approach can be easily modified or altered to better fit the problem at hand

examination will begin with 2-dimensional systems. The graphical simplicity of 2D systems facilitates the understanding of the procedure of this study while providing a basic insight into its necessity for systems with complex behavior. Figure 3 illustrates the trajectories of 3 important 2D systems and the corresponding Poincare sections, which were systematically selected. It can be visually confirmed that the Poincare sections associated with the proposed algorithm examine the attractors in detail and check all of their significant components. By utilizing such an approach and obtaining the corresponding Poincare maps, one can decisively talk about the qualitative (and in some cases, even quantitative) qualities of the attractor and its motion.

Figure 3a is a pedagogical trajectory, generated specifically to illustrate the importance of sections in examining the behavior of systems. As it can be observed, the top half of the trajectory illustrates aperiodic motion while its lower half indicates periodic motion. Consequently, an arbitrarily drawn Poincare section (red section in this case) might not provide valid interpretations of the dynamics of the system. In contrast, the Poincare sections of this algorithm (black sections in this case) will analyze all the pivotal components of the trajectory and provide insightful and correct interpretations. They even go as far as identifying the number of rotary flows and their centroids. The Duffing oscillator [10] and the Van der Pol oscillator [8] are also examined in Fig. 3 to further illustrate the capabilities of the proposed algorithm. The Van der Pol oscillator has the general formulation of study [8] with parameters $e = 0.5$, $B = 1$ and $w = 1$. The Duffing oscillator follows the format provided in study [10] with parameters $\delta = 0.02$, $\alpha_1 = 1$, $\alpha_2 = 5$, $l_0 = 8$ and $\Omega = 0.5$.

3.2 3D attractors and the significance of the geometrical approach

To elucidate the capabilities of this algorithm in treating all classes of systems, a number of 3D systems are discussed and examined. The Lorenz attractor is amongst the most investigated systems in chaos theory, and it is known that for certain parameters, the system falls into chaos [9] . The equation governing the motion of the Lorenz attractor is

$$\begin{cases} \dot{x} = \sigma(y - x) \\ \dot{y} = x(\rho - z) - y \\ \dot{z} = xy - \beta z \end{cases} \tag{17}$$

where $\sigma = 10$, $\rho = 28$ and $\beta = \frac{8}{3}$ for the simulations of this paper. Figure 5 illustrates the corresponding trajectory of the steady-state motion of this system and the systematically constructed Poincare sections. It should be noted that, the algorithm has identified the two rotary flows and drawn sections that cross all the important segments of the flow. The corresponding Poincare maps are also provided, which clearly illustrate the aperiodic motion. The point on the origin can be observed in every Poincare map of this paper but it should be noted that

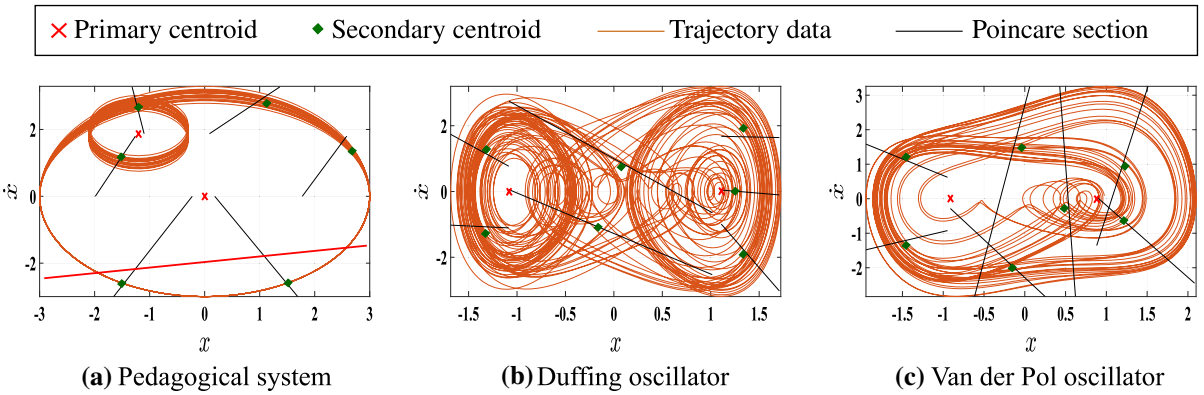

(a) Pedagogical system **(b)** Duffing oscillator **(c)** Van der Pol oscillator

Fig. 3 The Poincare sections are obtained for 3 important 2D attractors using the proposed algorithm: (a) the pedagogical system that illustrates different regimes of motion in different areas and the sensitivity of the interpretation of the qualitative behavior of the system to the geometry of the section ; (b) the trajectory of the Duffing oscillator corresponding to its steady-state motion and the Poincare sections of the proposed algorithm; (c) the trajectory of the Van der Pol oscillator corresponding to its steady-state motion and the Poincare sections of the proposed algorithm

this point is included in the Poincare map data due to an intended numerical procedure and does not actually belong to the Poincare map.

The next system of interest is Rossler's 3D attractor [14] which is known to be the simplest continuous system that can demonstrate chaotic motion. Nevertheless, the geometry of this attractor is different from that of the Lorenz and consequently, can be a good candidate for further examination of the effectiveness of this algorithm. The equation governing the motion of the Rossler's attractor is

$$\begin{cases} \dot{x} = -(y+z) \\ \dot{y} = x + ay \\ \dot{z} = b + x(z-c) \end{cases} \tag{18}$$

where $a = 0.1$, $b = 0.5$ and $c = 14$ for the simulations of this paper. Figure 5 shows Rossler's 3D attractor combined with the Poincare sections of this study. As it can be observed again, the sections are appropriately drawn and explore all the main segments of the flow. Aperiodicity can be observed in this motion as expected.

An alternative regime of motion that bears distinct qualitative behavior is quasi-periodicity. Quasi-periodic motion can be observed in a variety of dynamical systems, for example the orbits of certain celestial objects. More specifically, the restricted three body problem, discussed in study [7] can be considered as a good example to check the accuracy of the proposed methodology.

This class of systems usually has a trajectory in the form of a torus as depicted in Fig. 6. Additionally, it is known that the Poincare maps corresponding to quasi-periodic motion have continuously varying profiles. This can be readily observed in Fig. 6 as the methodology of this paper obtains optimal Poincare sections and computes the corresponding Poincare maps. As it can be seen, the Poincare maps all have a continuously varying profile with a defined shape signifies the qualitative quasi-periodicity of the motion.

The last 3D system of interest is the Rabinovich–Fabrikant attractor [3] which is known to illustrate a wide spectrum of motions including chaotic, periodic, strange nonchaotic, and transient chaotic. The equation governing the motion of the Rabinovich–Fabrikant attractor is

$$\begin{cases} \dot{x} = y(z-1+x^2) + ax \\ \dot{y} = x(3z+1-x^2) + ay \\ \dot{z} = -2z(b+xy) \end{cases} \tag{19}$$

where $a = 0.1$ and $b = 0.2875$ for the simulations of this paper. In this study, the parameters of this system are tuned to exhibit strange nonchaotic behavior that is seldom observed. Figure 7 illustrates the trajectory of this system and the provided Poincare sections. It should be noted that, the geometry of this attractor is fundamentally different from previously presented systems but nevertheless, the algorithm works flawlessly. The computed Poincare sections cross the attractor in all of its main segments and the aperiodicity of the behavior is apparent in the Poincare maps. Moreover,

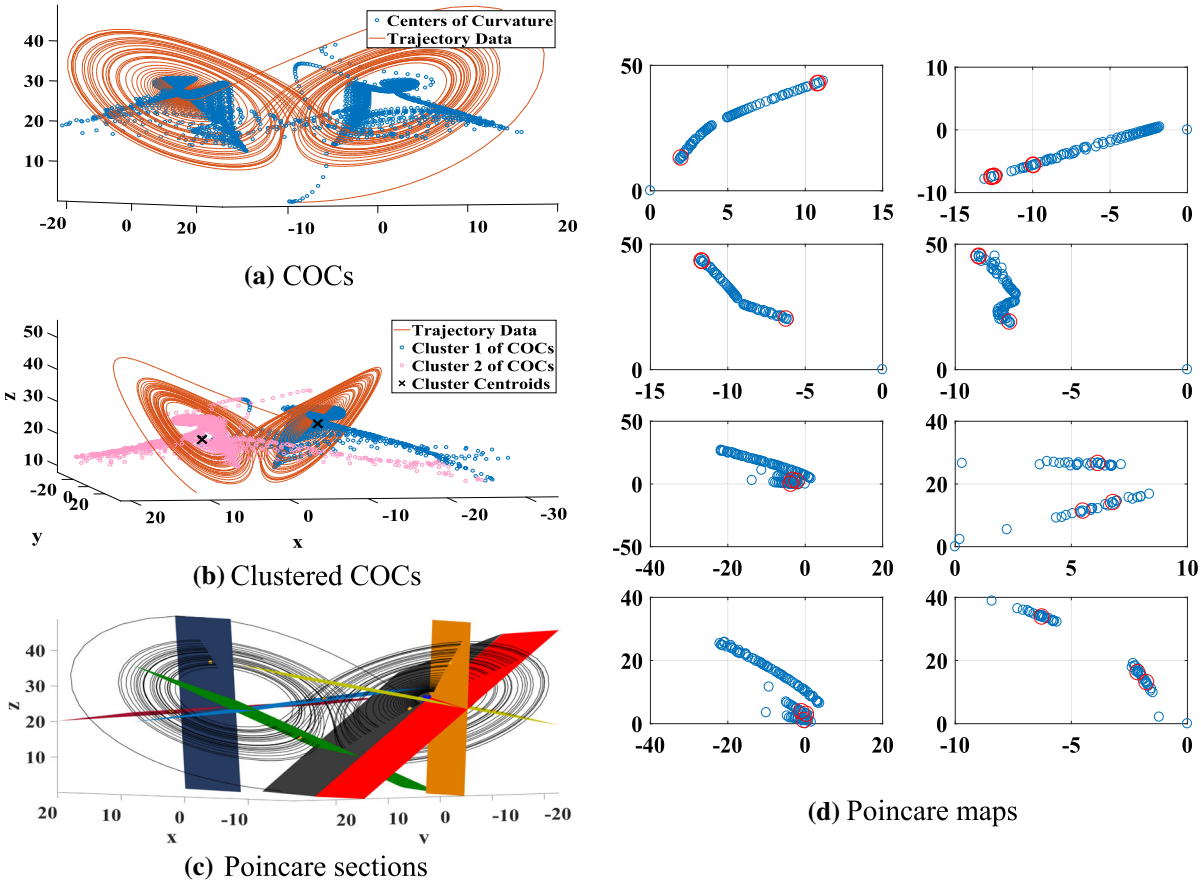

Fig. 4 The Poincare maps are obtained for the Lorenz attractor using the proposed algorithm: (a) the trajectory is depicted with the COC data that is within the limiting bounds and it can be observed that the COC data are concentrated in the centers of the rotary flows; (b) cluster analysis is performed and the COC data are segregated into two different clusters where each of their centroids is roughly located in the center of the rotary flows; (c) the corresponding Poincare sections are drawn and can examine all the pivotal sections of the trajectory; their corresponding Poincare maps can provide insightful information on the structure and behavior of the attractor and its periodicity; (d) the corresponding Poincare maps of the Lorenz attractor, where the red dots represent the last three intersections of the trajectory data with the Poincare section from which a state of aperiodicity can be concluded

the degree of aperiodicity is observed to be different in each section.

3.3 4D attractors and the extendibility of the algorithm to high dimensional systems

The proposed algorithm of this study can systematically provide effective Poincare sections irrespective of the dimensionality due to its use of fundamental geometry. To assess this capability, Rossler's 4D attractor [13] is examined and, the first 3D Poincare map is illustrated in Fig. 8. The equation governing the motion of Rossler's 4D (hyperchaotic) attractor is

$$\begin{cases} \dot{x} = -(y+z) \\ \dot{y} = x + ay + w \\ \dot{z} = b + xz \\ \dot{w} = -cz + dw \end{cases} \tag{20}$$

where $a = 0.25$, $b = 2.2$, $c = 0.5$, and $d = 0.05$ for the simulations of this paper. It is known that the attractor of interest demonstrates chaotic motion and the correspondingly obtained Poincare maps confirm this dynamic behavior.

An alternative 4D system that is particularly interesting is the 2DOF mass-spring-damper system subject to harmonic excitation and Coulomb friction and

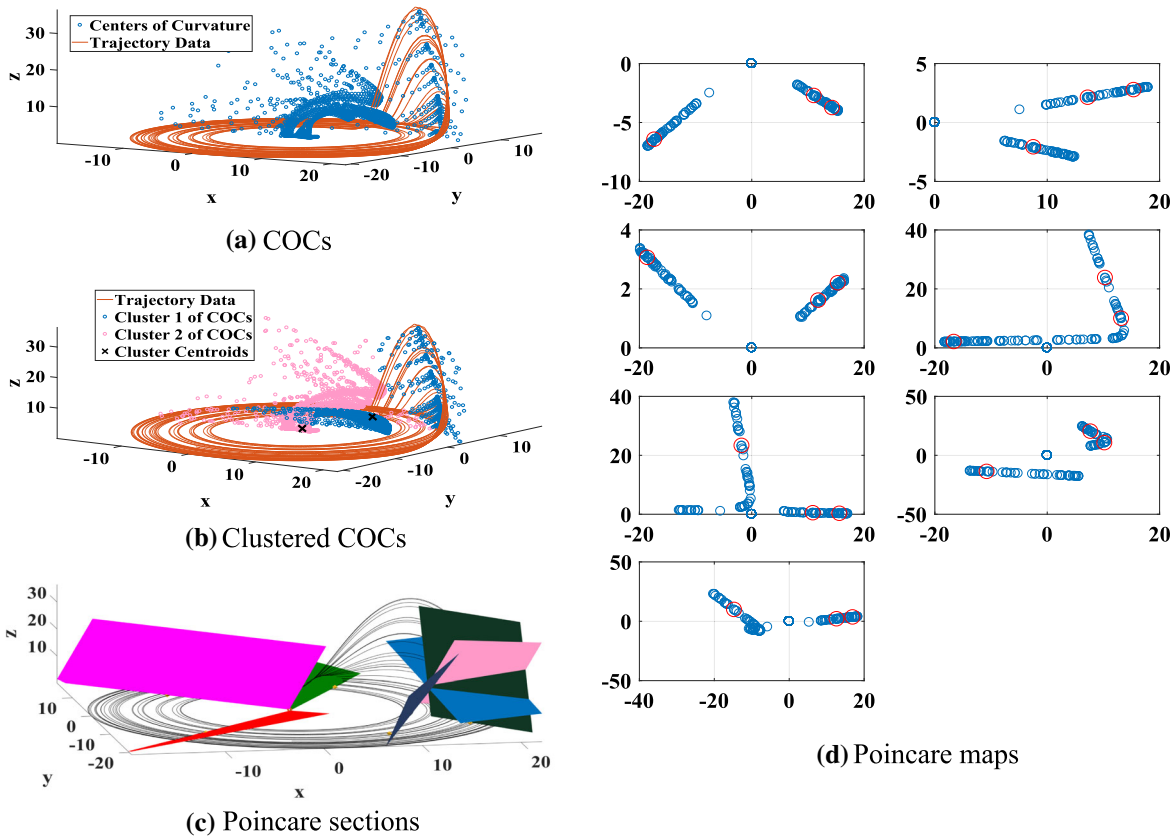

Fig. 5 The Poincare maps are obtained for the Rossler attractor using the proposed algorithm: (a) the trajectory is depicted with the COC data that is within the limiting bounds and it can be observed that the COC data are relatively concentrated in the centers of the rotary flows; (b) cluster analysis is performed and the COC data are segregated into two different clusters where each of their centroids is roughly located in the center of the rotary flows; (c) the corresponding Poincare sections are drawn and can examine all the pivotal sections of the trajectory; their corresponding Poincare maps can provide insightful information on the structure and behavior of the attractor and its periodicity; (d) the corresponding Poincare maps of the Rossler attractor, where the red dots represent the last three intersections of the trajectory data with the Poincare section from which a state of aperiodicity can be concluded

undergoing intermittent contact. The dynamics of this system is extensively discussed in the study [15] and the corresponding data are used here for convenience. The system can be reduced to four differential equations of order one and consequently, the corresponding full trajectory cannot be visualized. It is noteworthy to mention that this system can also be considered as five-dimensional if one takes into account time as a variable but since time, as a system variable, is monotonically increasing in trajectory space, its inclusion would not add any insight into the analysis and solely hinders the effective utilization of the Poincare map. Since the $x-y$ coordinates represent the motion of the first mass and the $z-w$ coordinates represent the motion of the second, the trajectories in $x-y$ represent the motion of the first mass and the trajectories in $z-w$ represents the motion of the second. It is important to note that, such physical interpretation is not always accessible for high-dimensional systems. Consequently, it would be interesting to see the Poincare map of this 4D system and compare it with the 2D trajectories of interest. Figure 9 illustrates this matter and it can be observed that the aperiodic motion is apparent in the Poincare maps. However, the detection of the aperiodicity of the motion is rather difficult to discern from its time response since the motion seems to be pseudo-periodic.

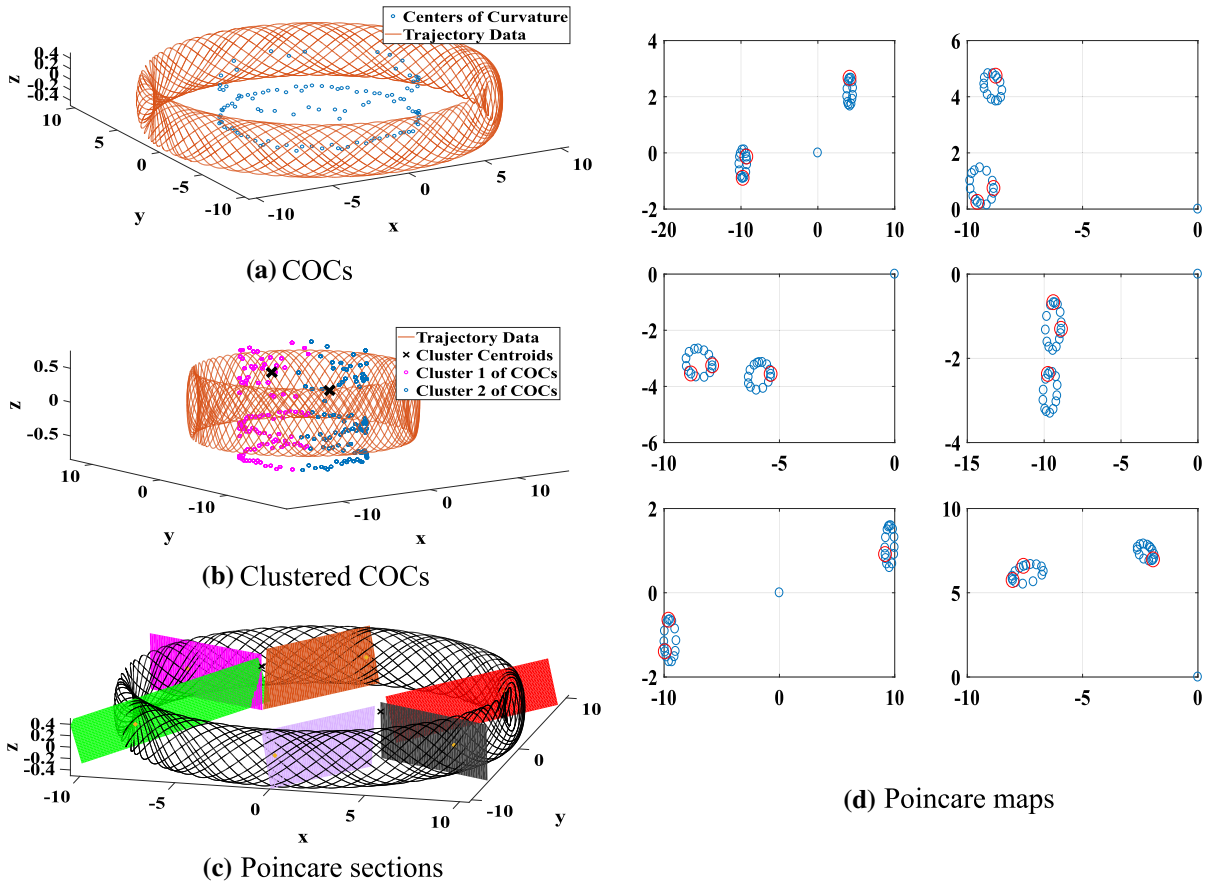

Fig. 6 The Poincare maps are obtained for a torus trajectory using the proposed algorithm: **a** the trajectory is depicted with the COC data that is within the limiting bounds and it can be observed that the COC data are relatively concentrated in the centers of the rotary flows; **b** cluster analysis is performed and the COC data are segregated into two different clusters where each of their centroids is roughly located in the center of the rotary flows; **c** the corresponding Poincare sections are drawn and can examine all the pivotal sections of the trajectory; their corresponding Poincare maps can provide insightful information on the structure and behavior of the attractor and its periodicity; **d** the corresponding Poincare maps of the torus trajectory, where the red dots represent the last three intersections of the trajectory data with the Poincare section from which a state of quasi-periodicity can be concluded

3.4 5D systems and statistical approaches

It is beneficial to conclude the examples of this paper with a 5D system to demonstrate the capabilities of the proposed methodology for higher dimensions. A 5D system has a 4D Poincare map that cannot be illustrated graphically. Nevertheless, it is possible to extract the Poincare map data and verify the regime of motion using statistical methods. The 5D example of this paper is borrowed from study [4] and is an extension of the famous Lorenz attractor. The governing equation of the system of interest is

$$\begin{cases} \dot{x} = \sigma(y - x) + u \\ \dot{y} = x(\rho - z) - y - v \\ \dot{z} = xy - \beta z \\ \dot{u} = -xz + k_1 u \\ \dot{v} = k_2 y \end{cases} \tag{21}$$

where $\sigma = 10$, $\rho = 28$, $\beta = \frac{8}{3}$, $k_1 = 2$ and $k_2 = 4$. After applying the methodology to the trajectory of this system, the Poincare map data corresponding to one of the Poincare sections is presented in Table 1.

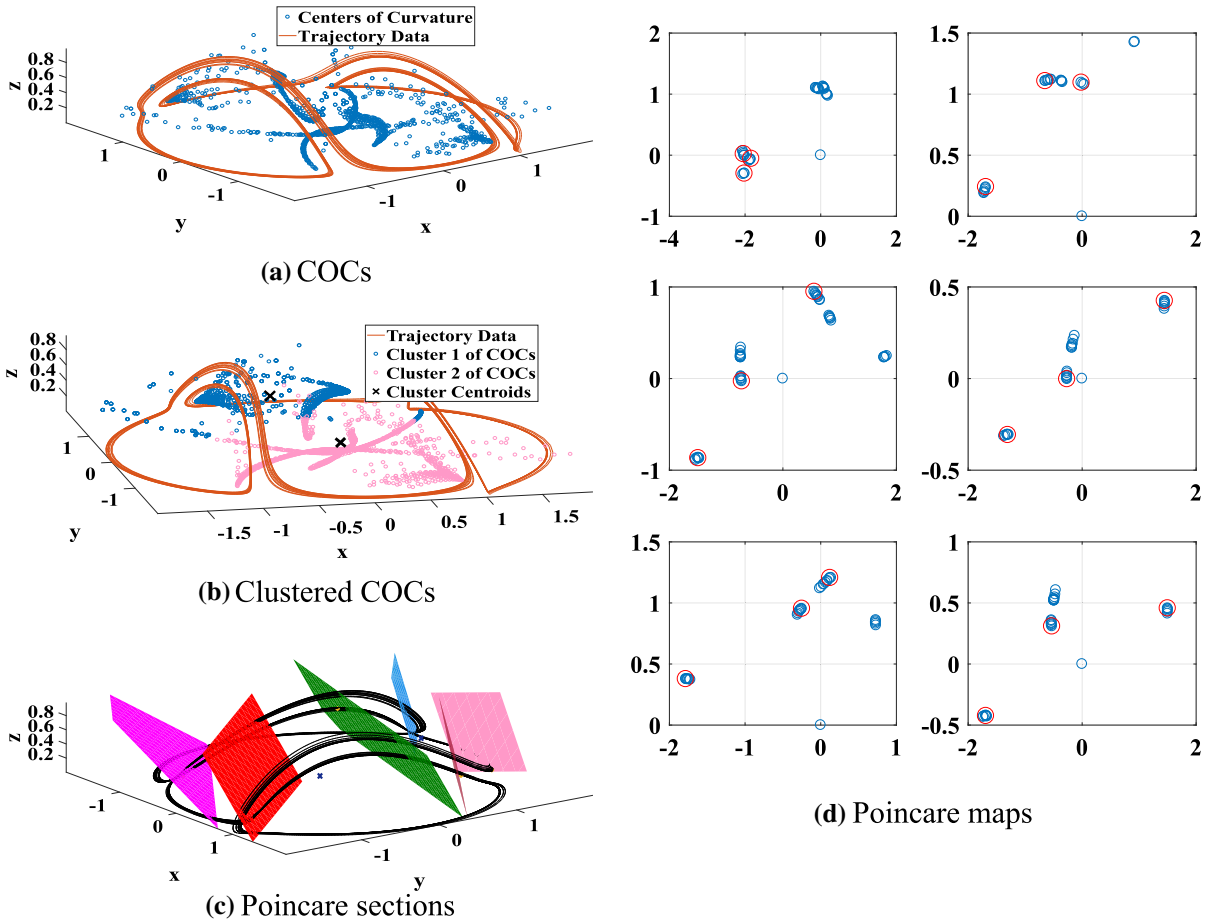

Fig. 7 The Poincare maps are obtained for the Rabinovich–Fabrikant attractor using the proposed algorithm: (a) the trajectory is depicted with the COC data that is within the limiting bounds and it can be observed that the COC data are relatively concentrated in the centers of the rotary flows; (b) cluster analysis is performed and the COC data are segregated into two different clusters where each of their centroids is roughly located in the center of the rotary flows; (c) the corresponding Poincare sections are drawn and can examine all the pivotal sections of the trajectory; their corresponding Poincare maps can provide insightful information on the structure and behavior of the attractor and its periodicity; (d) the corresponding Poincare maps of the Rabinovich–Fabrikant attractor, where the red dots represent the last three intersections of the trajectory data with the Poincare section from which a state of aperiodicity can be concluded

As it can be seen, the crossings do not show any repetitions and the Poincare map indicates aperiodic motion. It is also known from study [4] that this system is chaotic (or to be more accurate, hyperchaotic) and therefore, the results of the proposed methodology are in full agreement with the literature. The last three rows are highlighted as they are the most recent crossings and therefore, they should be compared with previous entries for any matchings. The $x'y'z'u'$ is the local coordinate system of the Poincare section.

4 Discussion

4.1 Variations and interpretations

The structure of the proposed algorithm of this study is very flexible and each of the utilized methods can be altered, substituted, and even reconstructed. The current methods are chosen to be as simple as possible to illustrate that even upon using such basic approaches, the method is quite effective. Nevertheless, it is possi-

Table 1 Location of Poincare section crossings for the 5D system indicate the aperiodicity of the motion

Data No.	x'	y'	z'	u'
1	−2.1454	9.8910	142.0184	−15.8692
2	−4.5678	28.7168	24.7632	−28.8906
3	7.3056	18.0953	−11.4636	−23.5760
4	−0.1015	44.2351	−174.9975	8.3729
5	2.4730	18.3785	88.4703	−26.7428
6	−1.9820	25.0820	−7.0682	−16.5508
7	5.4818	14.4770	−31.6606	−12.0346
8	−3.1961	30.2077	41.9489	−2.1878
9	−2.2562	13.2707	82.5215	−9.5441
10	−6.9411	19.8234	2.5983	0.0031
11	−0.3254	15.0098	141.4885	−25.2838
12	−5.4839	20.6275	58.6156	−18.8065
13	−1.3698	17.5126	56.0378	−18.5235
14	−4.1330	19.2838	−72.9641	1.6655
15	2.1076	17.8900	26.5670	−13.2827

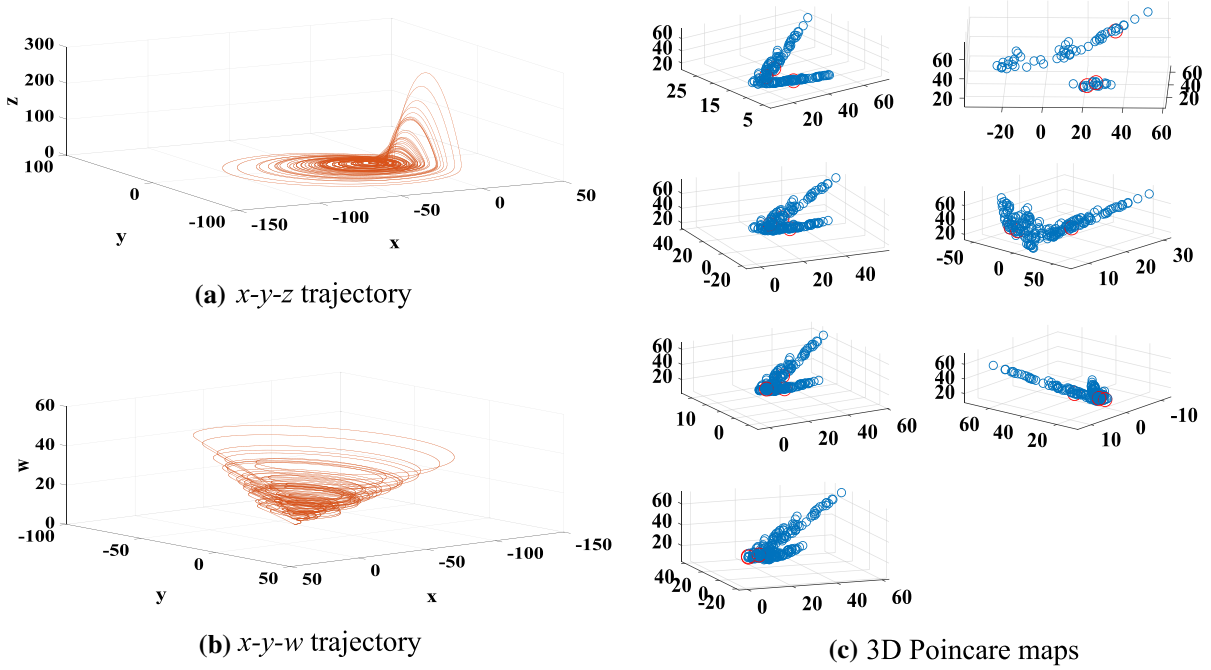

Fig. 8 The Poincare maps obtained for the 4D Rossler attractor using the proposed algorithm: (a) the $x-y-z$ components of the trajectory are depicted and the aperiodic motion of the system can be observed; (b) the $x-y-w$ components of the trajectory are illustrated to further signify the aperiodic motion of the attractor; (c) the corresponding 3D Poincare maps of the 4D Rossler attractor are obtained and the aperiodicity is apparent; the red dots represent the last three intersections of the trajectory with their corresponding Poincare sections and are highlighted to emphasize the aperiodicity of the motion

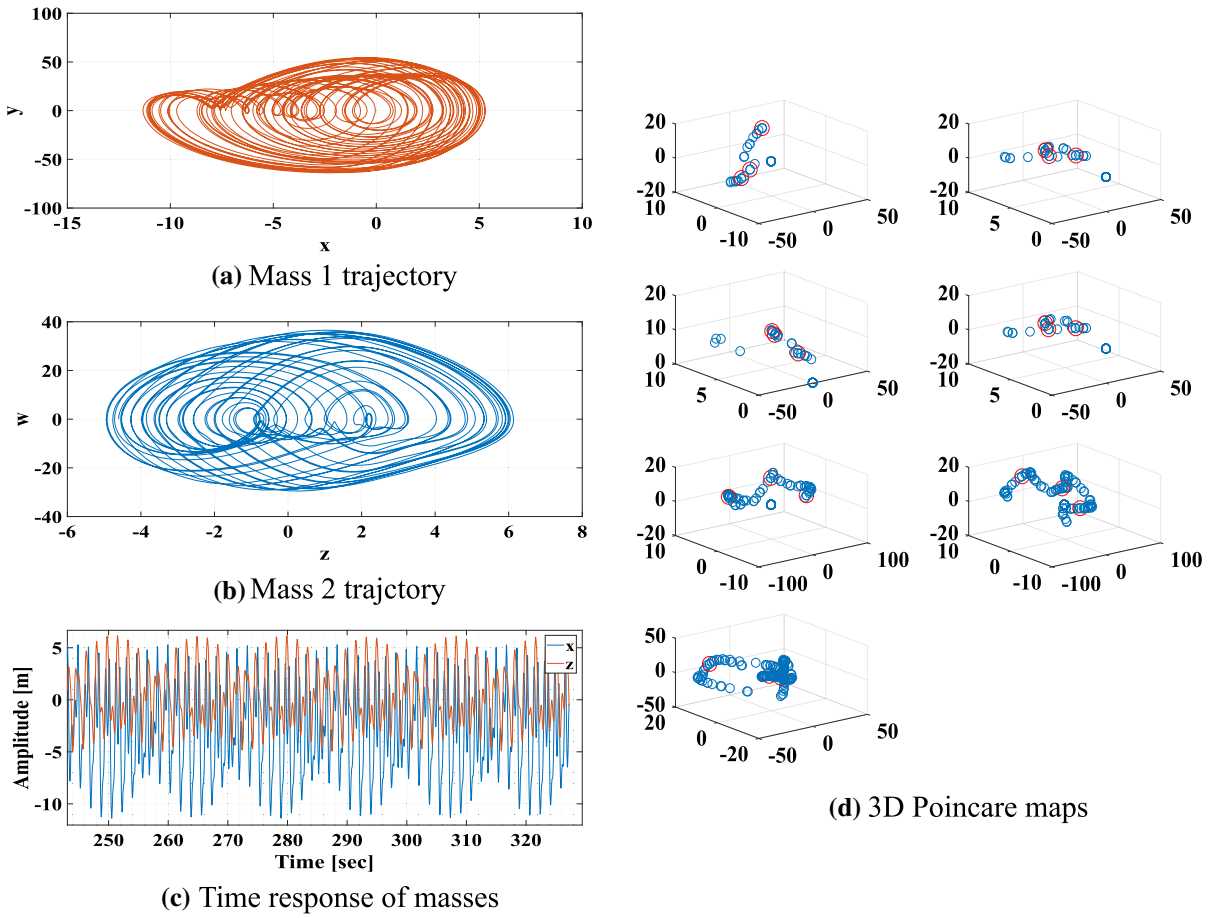

(a) Mass 1 trajectory

(b) Mass 2 trajctory

(c) Time response of masses

(d) 3D Poincare maps

Fig. 9 The Poincare maps are obtained for the 4D PWL attractor using the proposed algorithm; (a) the $x - y$ components of the trajectory are depicted but the aperiodic motion of the system cannot be conclusively observed; (b) the $z - w$ components of the trajectory are illustrated to demonstrate the motion of the second mass; (c) the time response of the system is shown for x and z and the aperiodicity is not apparent; (d) the corresponding 3D Poincare maps of the 4D PWL attractor are obtained and the aperiodicity is apparent; the red dots represent the last three intersections of the trajectory with their corresponding Poincare sections and are highlighted to emphasize the aperiodicity of the motion

ble to employ more sophisticated methods to elevate the level of accuracy or to orient the algorithm to a specific objective. For example, the clustering algorithm that is used in this work is the *k-means* clustering method [11] but upon using a more advanced clustering algorithm, such as the DBSCAN [6], it is possible to perform this process with more accuracy and even omit the outlier data to enhance the quality of the analysis. The statistical partitioning method of this algorithm can also be readily modified. For instance, the rudimentary statistical criteria of this study can be replaced by a more complex statistical method to obtain a more efficient partitioning algorithm. The focus of this study is on dynamical attractors using apposite Poincare sections but does not restrict researchers to specific methodologies that they need to employ to obtain these Poincare sections.

An additional topic, worthy of discussion, revolves around the relatively large number of sections. It might be thought that upon using a relatively large number of arbitrary sections, the structure of the attractor will be identified. Although this may be true for attractors with simple geometries, this randomized methodology faces critical issues in examining complex geometries. Bear in mind that the proposed algorithm evaluates all the rotary flows of the trajectory and investigates all its components in detail. This detailed systematic analysis was the primary intention of this algorithm that an arbitrary process of sectioning cannot match. Additionally, in the case of high dimensional systems, the problem

with arbitrary sections will be compounded since there would be no graphical basis for the selection.

An alternative discussion that might appear very beneficial is the difference between chaos and aperiodicity and the capability of conventional Poincare maps in determining each. Chaos is strictly defined as the exponential divergence of infinitesimally close trajectories in a bounded space while aperiodicity solely indicates a lack of periodic motion. In the 3D examples of this paper, Lorenz and Rossler's attractor were in fact, chaotic but the Rabinovich–Fabrikant attractor is nonchaotic while being strange and aperiodic. It is noteworthy to state that, despite the wide utilization of Poincare maps for chaos detection, this tool is only meant to examine periodicity and the existence of chaos should be separately evaluated using Lyapunov exponents. In this paper, the Poincare maps indicate that all the 3D examples are aperiodic but among them, only Lorenz and Rossler are chaotic and the Rabinovich–Fabrikant attractor is nonchaotic.

Additionally, it is impractical to identify chaos using a single Poincare section since the exponential divergence is not evident in a single section. To elucidate this matter, assume that a single Poincare section crosses a flow of trajectory data that corresponds to the folding stage of the chaotic motion of the corresponding attractor. In this particular section, it could be observed that all the crossings are rather compacted and differ very slightly. Nevertheless, it could be possible, and even intriguing, to assess the existence of chaos by the examination of Poincare map data of two consecutive sections in one stage.

It is noteworthy to state that the identification of aperiodic motion is much more apparent using a trajectory representation. The reason behind this convenience lies in the fact that in the graphical representation of one variable versus time, a long period is hardly distinguishable from pseudo-periodicity (when the motion is always very close to a periodic motion but has slight divergences, e.g., the Rabinovich–Fabrikant attractor). Nevertheless, in a trajectory representation, all the divergences of all the state variables are combined and the aperiodicity is more apparent. Consequently, a Poincare map can easily detect this aperiodicity.

An interesting manipulation of the structure of the current algorithm is to replace the idea of using simple hyperplanes as Poincare sections with more sophisticated hypersurfaces. The utilization of a hypersurface can ensure the satisfaction of all the Poincare section objectives and instead of finding a *close* answer, the algorithm can satisfy all the objectives simultaneously. That is, the hypersurface can go through both the primary and secondary centroids while being orthogonal to the average directionality vector. However, this approach substantially increases the level of computational effort and is only needed when the trajectory is exceptionally sophisticated.

4.2 Limitations

Due to the data-driven structure of the proposed methodology, the quality of the provided data critically affects the resulting Poincare maps. This section is devoted to discussing the possible issues and limitations that may influence this methodology and approaches that are available to bypass them.

The sampling rate of the flow is amongst the most influential properties and directly affects the quality of the resulting Poincare maps. The effects of sampling rate can be classified into two categories and discussed separately. The first category is concerned with obtaining the mapping after computing the trajectory and the Poincare section. In this case, it should be stated that a low sampling rate can exacerbate the accuracy of the Poincare maps to the point that the results are false. Nevertheless, this is not an issue specific to the proposed methodology and is the case for any numerical method that computes the Poincare map from trajectory data and a known section.

Alternatively, the second category is related to the computation of the Poincare section from the trajectory's raw data. The low sampling rate in this case will not significantly affect the clustering algorithms but might damage the quality of obtained centers of curvatures (CoCs) and ergo, mitigate the methodology's effectiveness. In contrast, the amount of data (as opposed to the sampling rate) is a significant factor in the cluster analysis of this methodology and a few thousand points is usually the minimum required dataset size. Moreover, the amount of data must be increased with an increase in dimensionality of the system to maintain the accuracy of the cluster analysis.

To demonstrate the effectiveness of the sampling rate in the calculation of the Poincare maps, the example of Fig. (6) is reconstructed using two different sampling rates for the case of a torus with periodic behavior.

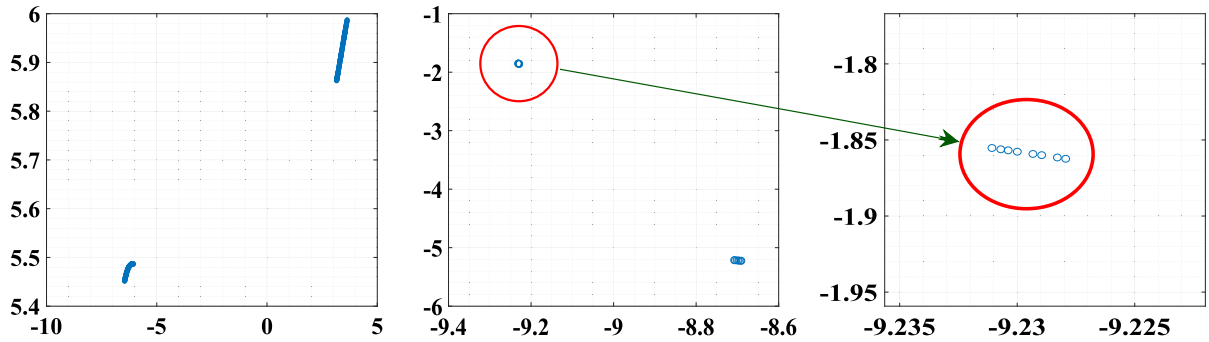

Fig. 10 The Poincare maps are obtained for the periodic torus trajectory using the proposed algorithm; **a** the resulting Poincare map for the system with a time increment of 0.01 seconds resulting in a very poor Poincare map; **b** the resulting Poincare map for the system with a time increment of 0.0005 seconds resulting in a very accurate Poincare map indicating the periodic nature of the motion; **c** the magnified view of the Poincare map with 0.0005 seconds time increment indicating slight variations as a result of numerical error

In the first scenario, the sampling rate is low and as it can be seen in Fig. (10a), the Poincare map (of one of the sections) falsely indicates a quasi-periodic motion. Nevertheless, by increasing the sampling rate to a reasonable value for this system, it can be observed that the system is clearly periodic in Fig. (10b). Notice that due to a change in the distribution of data, the Poincare sections also change and therefore, the Poincare maps are different. An additional insight that can be gained from this example is when one really zooms in on Fig. (10b) at a data point. This can be seen in Fig. (10c) the Poincare map data do not exactly coincide and there are slight variations in them even in the case of a decent sampling rate. These slight variations are the result of the implementation of the final linear interpolation to obtain the Poincare map data. Note that the two points that are right before and after the Poincare section are not identical at every iteration of the crossing. This, combined with the fact that the trajectory is not necessarily precisely a straight line near the section, causes these slight variations.

The next property of the raw data is the sampling uniformity. Contrary to the sampling rate, the sampling uniformity would not critically affect the outcome of this method unless its non-uniformity is rather extreme to the point that certain parts of the dynamics are neglected. Nevertheless, the non-uniformity of the raw data can be effective if the raw data are those that are in the immediate adjacency of the Poincare section. This means that if the data points that are just before and after the Poincare sections are non-uniform in a way that they are very close (and therefore with a higher accuracy), the resulting Poincare maps are more reliable and accurate. In contrast, if that non-uniformity causes the data in the adjacency of the Poincare section to be far apart, the quality of the Poincare sections is effectively reduced.

Finally, the proposed methodology might face certain issues if implemented on dynamical systems with discontinuous trajectories. Although this class of systems are rarely met in the world of engineering and usually belong to specific areas of mathematics, it is beneficial to address the possible issues for the sake of completeness. Initially, the discontinuity of the trajectory might undermine the quality of the CoCs significantly because the CoC profile will no longer be continuous. Furthermore, the Poincare sections are designed to pass through the primary and secondary centroids. The primary centroids usually have no part of the trajectory included and the main crossing of the trajectory and the section occurs at the secondary centroid. In the case of discontinuous trajectories, the secondary centroids might not also be where the trajectory data are aggregated but somewhere between them and the level of crossings, and consequently, the quality of the Poincare map, might drop.

5 Conclusion

This paper proposes a robust and effective methodology for selecting Poincare sections for dynamical systems that can examine the entirety of the trajectory and are effective irrespective of the level of the complexity

of the trajectory's geometry or its governing equations of motion. The methodology of this paper utilizes a geometrical-statistical approach to identify the structure of the trajectory to the point of rough reconstruction by determining the centers of rotary flows and the zones with the highest data concentration in each rotary flow. It then obtains a few Poincare sections that analyze the dynamical system in full without missing any major aspect of it.

to demonstrate the strength of this methodology in treating complicated nonlinear systems, various classical systems are examined, and the results are in agreement with existing knowledge. The systems studied include Lorenz, Rossler, Rabinovich–Fabrikant, Van der Pol, and the Duffing oscillator. It is also crucial to state that the structure of this methodology can be easily reconstructed or modified to further align it with the requirements of specific problems. In fact, the algorithms used in this paper are selected to be the simplest and the most rudimentary of their kind to offer a basic understanding of the methodology and to signify its effectiveness despite using basic tools.

Funding This paper is based on work partially supported by the National Science Foundation (United States) under Grant No. 1902408, program manager Dr. Harry Dankowicz, and the Ministry of Science and Technology (Taiwan, R.O.C) under Grant No. MOST 109-2222-E-007-006-MY3. Any opinions, findings, and conclusions or recommendations expressed in this paper are those of the authors and do not necessarily reflect the views of the National Science Foundation and the Ministry of Science and Technology.

Data Availability All the systems discussed in this work and the numerical values corresponding to their parameters are offered in the supplementary file. Additionally, the code for reproducing all the analysis is also attached, and can be used to investigate other systems as well.

Code availability The code for the proposed algorithm used to generate results in this work is also offered. The code is capable of treating all the systems that are compatible with the standard formulation used in this paper and can be downloaded from here. Please have in mind that improper choice of built-in parameters can result in erroneous results or syntax errors. The code can be downloaded from the resources section of the Nonlinear Dynamics and Vibration Laboratory's website at The Ohio State University.

Declarations

Conflicts of interest The authors have no conflicts of interest to declare that are relevant to the content of this article.

Consent to participate All the authors express their consent.

Ethics approval Not applicable

Consent for publication All the authors express their consent for the publication of this manuscript.

References

1. Barrio, R., Martínez, M.A., Serrano, S., Wilczak, D.: When chaos meets hyperchaos: 4d rossler model. Phys. Lett. A **379**(38), 2300–2305 (2015)
2. Brindley, J., Kapitaniak, T., El Naschie, M.: Analytical conditions for strange chaotic and nonchaotic attractors of the quasiperiodically forced Van der Pol equation. Phys. D Nonlinear Phenom. **51**(1–3), 28–38 (1991)
3. Danca, M.F., Kuznetsov, N.: Hidden strange nonchaotic attractors. Mathematics **9**(6), 652 (2021)
4. Hu, G.: Generating hyperchaotic attractors with three positive lyapunov exponents via state feedback control. Int. J. Bifurc. Chaos **19**(02), 651–660 (2009)
5. Kaas-Petersen, C.: Computation of quasi-periodic solutions of forced dissipative systems. J. Comput. Phys. **58**(3), 395–408 (1985)
6. Khan, K., Rehman, S.U., Aziz, K., Fong, S., Sarasvady, S.: DBSCAN: past, present and future. In: The fifth international conference on the applications of digital information and web technologies (ICADIWT 2014), pp. 232–238. (2014)
7. Kolemen, E., Kasdin, N.J., Gurfil, P.: Multiple poincare sections method for finding the quasiperiodic orbits of the restricted three body problem. Celest. Mech. Dyn. Astron. **112**(1), 47–74 (2012)
8. Ku, Y., Sun, X.: Chaos in van der pol's equation. J. Frankl. Inst. **327**(2), 197–207 (1990)
9. Lorenz, E.N.: Deterministic nonperiodic flow. J. Atmos. Sci. **20**(2), 130–141 (1963)
10. Luo, A.C., Han, R.P.: A quantitative stability and bifurcation analyses of the generalized duffing oscillator with strong nonlinearity. J. Frankl. Inst. **334**(3), 447–459 (1997)
11. MacQueen, J., et al.: Some methods for classification and analysis of multivariate observations. In: Proceedings of the fifth berkeley symposium on mathematical statistics and probability, Oakland, CA, USA. 281–297. (1967)

12. Month, L., Rand, R.H.: An application of the Poincare map to the stability of nonlinear normal modes (1980)
13. Rossler, O.: An equation for hyperchaos. Phys. Lett. A **71**(2–3), 155–157 (1979)
14. Rössler, O.E.: An equation for continuous chaos. Phys. Lett. A **57**(5), 397–398 (1976)
15. Shahhosseini, A., Tien, M.H., D'Souza, K.: Efficient hybrid symbolic-numeric computational method for piecewise linear systems with Coulomb friction. Available at SSRN 3940122 (2021)
16. Strogatz, S.H.: Nonlinear dynamics and chaos: with applications to physics, biology, chemistry, and engineering. CRC Press, Boca Raton, Florida (2018)
17. Tricoche, X., Schlei, W., Howell, K.C.: Extraction and visualization of Poincare map topology for spacecraft trajectory design. IEEE Trans. Vis. Comput. Gr. **27**(2), 765–774 (2020)
18. Tucker, W.: The lorenz attractor exists. C. R. de l'Acad des Sci. Ser. I-Math. **328**(12), 1197–1202 (1999)
19. Znegui, W., Gritli, H., Belghith, S.: Stabilization of the passive walking dynamics of the compass-gait biped robot by developing the analytical expression of the controlled Poincaré map. Nonlinear Dyn. **101**(2), 1061–1091 (2020)